

# Effects of substrate type and material-substrate bonding on high-temperature behavior of monolayer WS<sub>2</sub>

Liqin Su<sup>1</sup>, Yifei Yu<sup>2</sup>, Linyou Cao<sup>2</sup>, and Yong Zhang<sup>1</sup> (✉)

<sup>1</sup> Department of Electrical and Computer Engineering, University of North Carolina at Charlotte, Charlotte, 28262, USA

<sup>2</sup> Department of Materials Science and Engineering, North Carolina State University, Raleigh, 27695, USA

**Received:** 22 January 2015

**Revised:** 23 March 2015

**Accepted:** 29 March 2015

© Tsinghua University Press  
and Springer-Verlag Berlin  
Heidelberg 2015

## KEYWORDS

tungsten disulfide,  
high temperature,  
Raman,  
temperature coefficient,  
photoluminescence,  
activation energy

## ABSTRACT

This study reveals that the interaction between a 2D material and its substrate can significantly modify its electronic and optical properties, and thus can be used as a means to optimize these properties. High-temperature (25–500 °C) optical spectroscopy, which combines Raman and photoluminescence spectroscopies, is highly effective for investigating the interaction and material properties that are not accessible at the commonly used cryogenic temperature (e.g., a thermal activation process with an activation of a major fraction of the bandgap). This study investigates a set of monolayer WS<sub>2</sub> films, either directly grown on sapphire and SiO<sub>2</sub> substrates by CVD or transferred onto SiO<sub>2</sub> substrate. The coupling with the substrate is shown to depend on the substrate type, the material-substrate bonding (even for the same substrate), and the excitation wavelength. The inherent difference in the states of strain between the as-grown and the transferred films has a significant impact on the material properties.

## 1 Introduction

Following the discovery of two-dimensional (2D) materials, such as graphene and boron nitride [1–4], graphene analogues of other layered materials with a similar hexagonal structure, especially those compounds involving transition metal dichalcogenides (TMDs) [5], have recently attracted significant attention due to their various physical, chemical, and mechanical properties for use in various applications [6–13]. The basic building block of TMDs consists of one atomic layer of transition metal atoms in between two

chalcogen atomic layers. Together, referred to as one monolayer (1L), is shown in Fig. 1(a). Bulk TMD crystals are semiconductors with an indirect band gap in the near infrared spectral range, while monolayer TMDs, such as molybdenum disulfide (MoS<sub>2</sub>), tungsten disulfide (WS<sub>2</sub>), or tungsten diselenide (WSe<sub>2</sub>), have a direct band gap in the visible spectral range. This is in contrast to graphene's zero gap and monolayer hexagonal boron nitride's (h-BN) large gap of > 5 eV [13–16]. Besides their indirect-to-direct bandgap transition with the reducing number of layers, the monolayer or 2D transition metal disulfides 2D-MS<sub>2</sub> (M = W, Mo),

Address correspondence to [yong.zhang@uncc.edu](mailto:yong.zhang@uncc.edu)

which have been intensively studied among the 2D-TMDs, exhibit a high carrier mobility of approximately  $200 \text{ cm}^2/(\text{V}\cdot\text{s})$ , strong spin-orbit coupling, and weak room temperature (RT) ferromagnetism [17–21]. Therefore, 2D- $\text{MS}_2$  has broad potential for next-generation electronic and optical device applications, such as flexible heterostructures of graphene- $\text{WS}_2$  for field effect tunneling transistors [22, 23].

However, with very few exceptions, the reported properties of TMDs were obtained with the film supported by a substrate. A well-known effect of the substrate includes charge doping, which often results in changes in the peak position and intensity of a spectral feature (e.g., in Raman and photoluminescence spectroscopies) [24, 25]. Another effect is a change in dielectric environment, which affects the optical contrast of the film against the substrate and further leads to an optical interference effect that can affect the signal strength of the spectroscopy feature [26]. These studies were typically done with mechanically exfoliated and transferred films. We have recently discovered a more subtle substrate effect with  $\text{MoS}_2$  [27]. The film-substrate interaction depends on the mesoscopic film morphology that in turn depends on

whether the film is grown directly or mechanically transferred onto the substrate. The difference in film morphology leads to drastically different temperature shifts for the in-plane and out-of-plane lattice vibration modes. This finding suggests that the surface morphology difference could significantly impact the in-plane electronic transport through electron-phonon coupling, which is sensitive to the symmetry of the vibration mode [28]. We suggest that in contrast to cooling the sample to cryogenic temperature, heating the film to material decomposition temperature can provide further insight to the film-substrate interaction for the following considerations. (1) At an elevated temperature the film is more likely to re-arrange its bonding with the substrate, which is relevant to the annealing effect. (2) It may be possible to evaluate the effect of the built-in strain associated with the thermal expansion coefficient (TEC) mismatch between the film and substrate after cooling from the growth temperature. (3) The ability to study thermal activation processes that exhibit larger activation energies than RT can offer. (4) The actual operating temperature of a thin-film device is often substantially higher than the intended RT. Most of these points are, in fact,

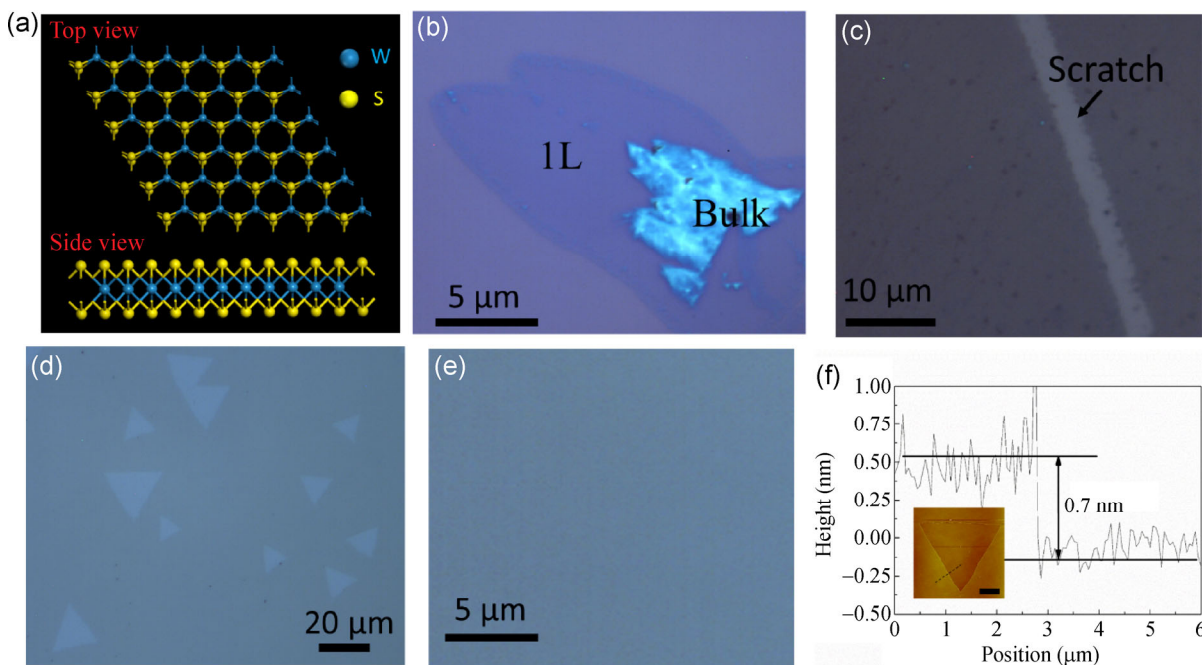


**Figure 1** (a) Schematic model of  $\text{WS}_2$  single layer with top and side views. (b)–(e) Optical images of  $\text{WS}_2$  samples: (b) 1L- $\text{SiO}_2$  and bulk- $\text{SiO}_2$ , (c) 1L-TRAN- $\text{SiO}_2$ , (d) 1L-SA-TRI, and (e) 1L-SA-FILM. (f) AFM image of 1L  $\text{WS}_2$  triangle on sapphire, with a thickness of 0.7 nm.

more relevant for the 2D materials than traditional 3D materials, because the nature of the film-substrate bonding is very different. As a consequence, heat dissipation in the 2D material is very different and challenging, e.g., the issue of self-heating in a WS<sub>2</sub> based device [23]. This type of study may eventually allow us to understand the intrinsic properties of the ideal freestanding, 2D material by extrapolating the results obtained with the substrate.

Raman spectroscopy is a nondestructive technique used to characterize the structural and electronic properties of monolayer materials such as graphene and MoS<sub>2</sub> [27, 29]. It was recently shown that this technique is suitable for a quick determination of the number of monolayers in WS<sub>2</sub>, in a similar manner as in MoS<sub>2</sub>, by the dependence of Raman peak positions on the number of layers [30, 31]. Temperature-dependent photoluminescence (PL) spectroscopy is often used to investigate radiative and non-radiative recombination processes and exciton-phonon interactions in semiconductor materials. In general, thermal quenching of the PL intensity with increasing temperature can be attributed to the thermal activation of defects or impurities. Such a study is usually performed in the temperature range from cryogenic to RT. Higher temperatures, in principle, would allow us to examine an impurity state with a larger activation energy. However, this technique has rarely been applied above RT. This is because the PL signal is thought to become very weak at higher temperatures, even for a bulk material that offers a large absorption volume. For this reason, the high-temperature measurements are expected to be more challenging for a single monolayer material like WS<sub>2</sub>.

In this work, we perform temperature-dependent PL and Raman investigations on a set of single monolayer WS<sub>2</sub> samples with temperatures up to 500 °C (near the decomposition point). Both Raman and PL measurements indicate the existence of significant coupling between the 2D-WS<sub>2</sub> and its substrate, in contrast to the common assumption that the substrate merely provides mechanical support and that most properties are intrinsic to the film. Not only do the effects of the substrate vary drastically between the as-grown films on SiO<sub>2</sub> and sapphire substrates, but also the substrate effects are different between the as-

grown and the transferred films on the same substrate type. Beyond the well-known doping effect caused by the chemical residual on the transferred film [32, 33], we demonstrate that the inherent difference in the states of strain between the as-grown and transferred films has a major impact on the material properties. The substrate effect may tune the band structure of WS<sub>2</sub> monolayers, manifesting itself as changes in the optical properties, such as Raman enhancement, PL peak energy, and their temperature dependencies. The PL measurements also show a major difference in both RT PL intensity and thermal quenching processes between the samples grown on different substrates. For the 2D-WS<sub>2</sub> on SiO<sub>2</sub>, a thermal quenching process with an activation energy of 0.40 eV was observed, whereas on sapphire, two thermal quenching processes were observed, with activation energies of 0.20 and 1.51 eV, respectively.

## 2 Experimental

In a previous study, we demonstrated the growth of a large-area single crystalline monolayer WS<sub>2</sub> [34], and a technique to transfer the large film as a whole to a secondary substrate [35]. These developments make the current study possible. Five samples were studied in this work, as follows. (a) “1L-SiO<sub>2</sub>” is a monolayer WS<sub>2</sub> film grown on Si substrate coated with 300 nm SiO<sub>2</sub>. (b) “1L-SA-TRI” is a triangular-shaped monolayer WS<sub>2</sub> film, grown on sapphire substrate. (c) “1L-SA-FILM” is a large area monolayer WS<sub>2</sub> film grown on sapphire substrate. (d) “1L-TRAN-SiO<sub>2</sub>” is a transferred monolayer WS<sub>2</sub> film originally grown on sapphire. (e) “Bulk-SiO<sub>2</sub>” is a thick layer of WS<sub>2</sub> (> 20 monolayers) on the same SiO<sub>2</sub>/Si substrate as “1L-SiO<sub>2</sub>”. Figures 1(b)–1(e) show the optical images of the four samples, with an AFM image of 1L-SA-TRI shown in Fig. 1(f). The thickness of the 1L WS<sub>2</sub> was measured to be ~0.7 nm, consistent with the expected thickness of the monolayer [36].

Raman and PL measurements were carried out in a Horiba LabRAM HR800 Micro-Raman system in back-scattering geometry with a spectral resolution better than 1 cm<sup>-1</sup>. The temperature-dependent measurements were carried out with a 50× long-working-distance lens (NA = 0.5). A Linkam TS1500 heating system, with

a temperature accuracy of  $\pm 1^\circ\text{C}$ , was used to heat the samples at increments of  $25^\circ\text{C}$  and a heating rate of  $10^\circ\text{C}/\text{min}$ . Before acquiring the spectrum, the temperature was held for at least five minutes at each temperature, allowing sufficient time for stabilization. To prevent the  $\text{WS}_2$  films from reacting with oxygen, a low flow rate of nitrogen gas was purged through the sample chamber. A sufficiently low laser power ( $< 1\text{ mW}$ ) was used to minimize sample heating. Two excitation wavelengths were used, 532 and 441.6 nm, to examine the excitation wavelength dependence for near-resonance and off-resonance excitation.

### 3 Results and discussion

#### 3.1 The effect of substrate type and wavelength on room temperature Raman and PL

Figures 2(a)–2(e) show typical Raman spectra of all four 1L samples as well as “bulk”  $\text{WS}_2$  under both 532 and 441.6 nm laser excitation. The corresponding excitation energies were near and off resonant with the B exciton of the material, respectively. A laser power of  $\sim 150\ \mu\text{W}$  was used. Under 441.6 nm excitation,

the four 1L samples exhibited similar spectroscopy features in the spectral region of interest: two optical modes,  $E_{2g}^1(\Gamma)$  for the in-plane motion of W + S atoms at  $\sim 355\text{ cm}^{-1}$  and  $A_{1g}(\Gamma)$  for the out-of-plane motion of two S atoms at  $\sim 417\text{ cm}^{-1}$ , separated by  $61.7\text{ cm}^{-1}$ . The  $E_{2g}^1(\Gamma)$  and  $A_{1g}(\Gamma)$  separation has been shown to be a simple signature for the monolayer  $\text{WS}_2$  [30]. For the “bulk”  $\text{WS}_2$ , the frequency difference between the  $E_{2g}^1(\Gamma)$  and  $A_{1g}(\Gamma)$  modes was  $65\text{ cm}^{-1}$ . The two on-sapphire samples showed comparable Raman intensities, whereas the 1L- $\text{SiO}_2$  sample produced a lower signal by a factor of 2–3, but the transferred sample 1LTRAN- $\text{SiO}_2$  has the strongest signal,  $\sim 3$  times that of the on-sapphire samples.

Under near-resonant excitation of 532 nm, a few additional Raman peaks appeared on the lower frequency side of the  $E_{2g}^1(\Gamma)$ ; in particular, a very strong second order peak 2LA(M) almost overwhelms the  $E_{2g}^1(\Gamma)$ . A fitting procedure is required to deconvolute the 2LA(M) and  $E_{2g}^1(\Gamma)$  components. The resonant effect also produced very rich Raman modes in the lower (frequency region and some additional features in the higher frequency region (Fig. S1 in the Electronic Supplementary Material (ESM)) [31]. The most striking

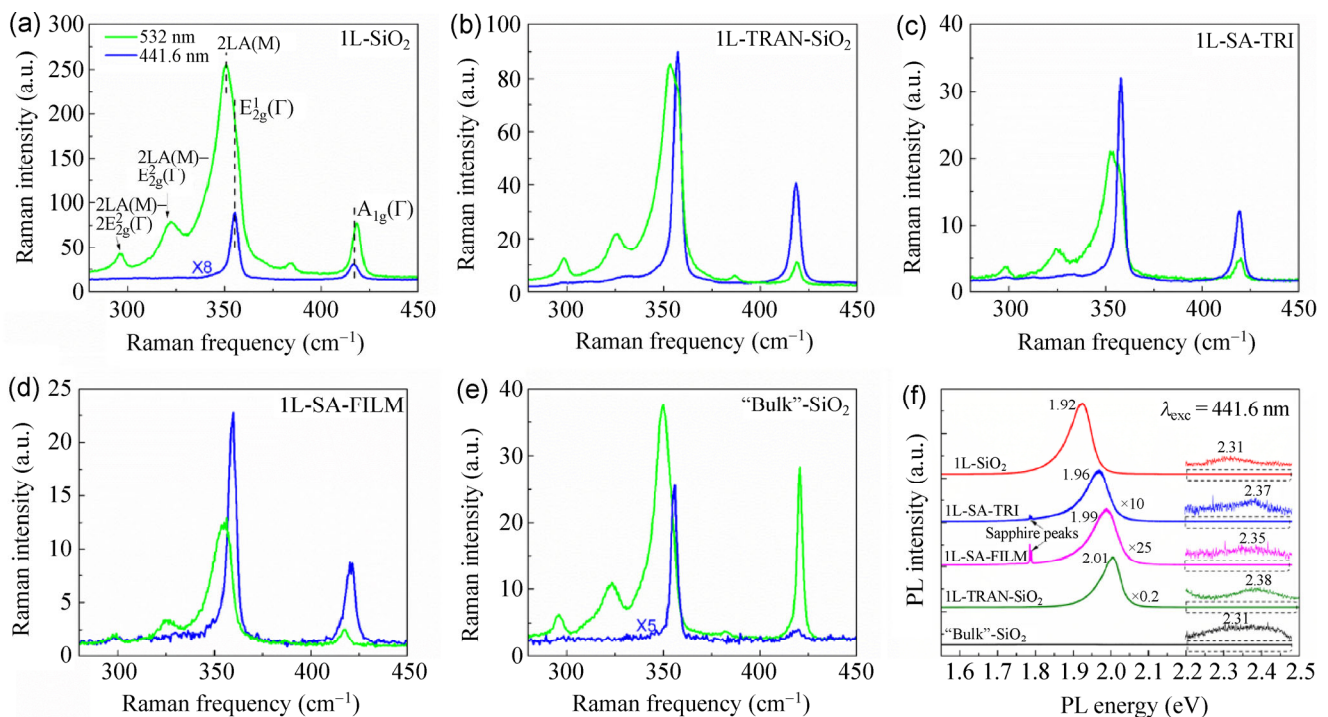


**Figure 2** (a)–(f) Raman and PL of all five  $\text{WS}_2$  samples with excitation wavelengths of 441.6 nm (blue line) and 532 nm (green line). (f) PL with 441.6 nm excitation.

observation seen when comparing the four 1L samples was that the signals of the on-SiO<sub>2</sub> samples, both the as-grown and the transferred, were substantially stronger than those of the other two on-sapphire samples. In particular, the 1L-SiO<sub>2</sub> was stronger by over a factor of 10–20, and the 1L-TRAN-SiO<sub>2</sub> by a factor of 3–5. The three as-grown samples indicated an anti-correlation between the resonant and the off-resonant signals, i.e., a stronger resonant signal under 532 nm excitation corresponded to a weaker off-resonant signal under 441.6 nm excitation. The transferred film on SiO<sub>2</sub> showed the strongest off-resonant signal, which was approximately 10 times that of the as-grown sample on the same type of substrate and approximately 3 times weaker under near-resonant excitation. These comparisons offer the first indication of substrate and film-substrate bonding dependence of the 2D-WS<sub>2</sub> film, and that more than one mechanism is at work to produce these substrate effects. The relative intensities of the samples at two excitation wavelengths are summarized in Table 1.

We then analyzed the substrate effect on the electronic structure. Monolayer WS<sub>2</sub> had two interband transitions near the bulk direct transitions at the K point due to spin-orbit splitting of the valence band, assigned as A (1.95 eV) and B (2.36 eV) excitons [12, 37]. Figure 2(f) shows PL spectra of all the WS<sub>2</sub> samples excited with 441.6 nm. In our samples, a weak peak at ~2.35 eV, corresponding to the B exciton, was seen at RT, which indicated the high quality of the CVD-grown 1L WS<sub>2</sub>. The primary PL band near the fundamental bandgap exhibited significant asymmetric broadening on the lower energy side, which can be deconvoluted into two components using two Gaussian line-shape functions, as shown in Fig. S2 (in the ESM). The higher

energy component was attributed to the A exciton of the fundamental bandgap, whereas the lower energy component was interpreted as a negatively charged exciton (A<sup>-</sup>), also known as a trion. Trions results from n-type doping due to either charge transfer from the substrate or defects in the film [38, 39]. The variation in the A exciton peak position among these samples is likely due to strain. For the CVD grown samples, if we assume that the 2D film is deposited on the substrate with very little strain at the growth temperature (typically 900 °C), after cooling to RT, the difference in TEC between the film and substrate will introduce strain in the film. The TECs of both SiO<sub>2</sub> and sapphire are less than that of WS<sub>2</sub> [40, 41], with SiO<sub>2</sub> being much less than that of WS<sub>2</sub> and sapphire being near that of WS<sub>2</sub>. This suggests that more tensile strain is generated in the WS<sub>2</sub> film grown on SiO<sub>2</sub> than on sapphire, leading to the largest redshift of the PL peak energy in the 1L-SiO<sub>2</sub> sample. However, for the transferred sample 1L-TRAN-SiO<sub>2</sub> on the same type of substrate as 1L-SiO<sub>2</sub>, the PL exhibited the highest peak energy. It is suggested that the strain is released after being transferred. The high lying B-exciton state is less affected by the impurities and defects that are likely to contribute to the band edge emission. The fact that the B-exciton transition energies follow quite closely those of the band edge emission supports the interpretation that the PL peak shift is due to the strain effect. Based on the PL peak position difference between 1L-SiO<sub>2</sub> and 1L-TRAN-SiO<sub>2</sub> and their theoretically calculated bandgap deformation potential (-0.19 eV/% for tensile strain, using density functional theory (DFT) [42]), the built-in epitaxial strain in 1L-SiO<sub>2</sub> can be estimated to be 0.47%.

The PL intensity of 1L-TRAN-SiO<sub>2</sub> is stronger than 1L-SiO<sub>2</sub> by a factor of 5, which is in contrast to the relative intensity in Raman, where 1L-SiO<sub>2</sub> is stronger. The small bandgap shift should not significantly affect PL intensity, because of the typically weak absorption strength variation with wavelength. There are two known major effects influencing the intensity of band edge PL emission: (1) doping [24, 25], and (2) optical interference [26]. It is suggested that the stronger bonding for the as-grown sample quenches the PL relative to the transferred sample with weaker bonding to the otherwise same SiO<sub>2</sub> substrate. However, the

**Table 1** Relative intensities of Raman and PL of four monolayer WS<sub>2</sub> samples measured at two excitation wavelengths: 532 and 441.6 nm. For each column, the weakest intensity represents unity

	532 nm		441.6 nm	
	Raman	PL	Raman	PL
1L-SiO <sub>2</sub>	20	7.5	1.0	25
1L-TRAN-SiO <sub>2</sub>	7.3	300	10	125
1L-SA-TRI	1.7	1.5	3.3	2.5
1L-SA-FILM	1.0	1.0	2.3	1.0

PL intensities of the on-SiO<sub>2</sub> samples are stronger than the on-sapphire samples. For example, the PL intensity of 1L-TRAN-SiO<sub>2</sub> is 125 times that of 1L-SA-FILM. The PL intensity reduction for the on-sapphire samples may be due to non-radiative recombination via the substrate. Additionally, the interference effect of the thin-layer SiO<sub>2</sub> could slightly enhance the light absorbed by the WS<sub>2</sub> film and its collection efficiency [26]. Qualitatively similar substrate type dependence was also observed for 532 nm excitation (Fig. S2 in the ESM). The relative PL intensities are summarized in Table 1. In short, the SiO<sub>2</sub> substrate offers much stronger PL than sapphire substrate for both excitation wavelengths. These observations illustrate that film-substrate interaction can be complex.

The effect of the wavelength-dependent substrate in Raman intensity is shown in Figs. 2(a)–2(e). For 1L-SiO<sub>2</sub>, the 532 nm excitation yielded a much stronger 2LA(M)/E<sub>2g</sub><sup>1</sup>(Γ) Raman signal than 441.6 nm, which is in stark contrast to 1L-SA-TRI and 1L-SA-FILM. In these latter two samples, 441.6 nm excitation yielded stronger signals than 532 nm excitation did. The strong 1L-SiO<sub>2</sub> intensity enhancement under 532 nm excitation can be explained by the resonant Raman effect described below (Eq. (1)) [43]

$$I(E_L) = K \left| \frac{\langle f | H_{e-r} | b \rangle \langle b | H_{e-ph} | a \rangle \langle a | H_{e-r} | i \rangle}{(E_L - E_g - i\Gamma_a)(E_L - E_{ph} - E_g - i\Gamma_b)} \right|^2 \quad (1)$$

where  $I(E_L)$  is the Raman scattering intensity, and  $K$  is a constant.  $|i\rangle$  is the initial state,  $|a\rangle$  and  $|b\rangle$  are two intermediate states, and  $|f\rangle$  is the final state.  $H_{e-r}$  and  $H_{e-ph}$  are the Hamiltonians of the radiation of the light and the electron-phonon coupling, respectively.  $E_L$  is the energy of the incident light,  $E_g$  is the energy of the electronic transition, and  $E_{ph}$  is the phonon energy.  $\Gamma_a$  and  $\Gamma_b$  are the damping constants related to the lifetimes of the two intermediate states  $|a\rangle$  and  $|b\rangle$ , respectively.

The 532 nm excitation wavelength (2.33 eV) was very close to the energy of B exciton to yield Resonant Raman scattering. The first term in the denominator of Eq. (1) reflects the resonance of the incoming photon with the B exciton transition energy, and the second term reflects the resonance of the outgoing photon with the phonon energy. The B-exciton PL

emission energy of 1L-SiO<sub>2</sub> at 2.31 eV was the closest to the laser energy among the four 1L samples. This suggests that the incoming electronic resonant plays a dominant role. The resonant effect was shown to become progressively weaker with decreasing excitation wavelength [31]. The difference in Raman intensity between the two on-SiO<sub>2</sub> samples under 532 nm excitation could be explained by the energy change from the resonance condition due to the difference in their B exciton energy levels (2.31 vs. 2.38 eV). However, the Raman intensity difference under 441.6 nm could be caused by another mechanism that has yet to be determined. One possibility could be the difference in charge transfer or doping.

### 3.2 High-temperature Raman scattering

A temperature-dependent Raman study was reported on for a 1L mechanically exfoliated (ME) WS<sub>2</sub> from 77 to 623 K with temperature coefficients of both E<sub>2g</sub><sup>1</sup>(Γ) and A<sub>1g</sub>(Γ) modes being  $-0.006 \text{ cm}^{-1}/\text{K}$ . However, the temperature data were non-linear [44]. As shown previously for MoS<sub>2</sub>, ME film is expected to have very different bonding with the substrate, compared to that of the epitaxial film [27, 45]. Here we performed the high-temperature Raman investigations for the four 1L WS<sub>2</sub> samples from RT to 500 °C. Figure 3(a) shows the temperature-dependent Raman spectra of 1L-SiO<sub>2</sub>. For both E<sub>2g</sub><sup>1</sup>(Γ) and A<sub>1g</sub>(Γ) modes, the Raman frequency decreased with increasing temperature. In addition, the intensity of 2LA(M) decreased significantly as the temperature increased. This is because the bandgap redshift detunes the laser energy from resonance. Empirically, the temperature dependence of Raman shift can be expressed as (Eq. (2))

$$\omega(T) = \omega_0 + \chi_1 \Delta T + \chi_2 (\Delta T)^2 + \chi_3 (\Delta T)^3 \quad (2)$$

where  $\omega_0$  is the frequency at RT,  $\Delta T$  is the temperature change relative to RT, and  $\chi_1$ ,  $\chi_2$  and  $\chi_3$  are the first-, second- and third-order temperature coefficients, respectively. Note that one of the sapphire Raman peaks at  $417 \text{ cm}^{-1}$  overlaps with the WS<sub>2</sub> A<sub>1g</sub>(Γ) peak. Thus, the sapphire samples' spectra were collected at each temperature and carefully subtracted to yield the WS<sub>2</sub> Raman spectrum, as illustrated in Fig. S3 (in the ESM).

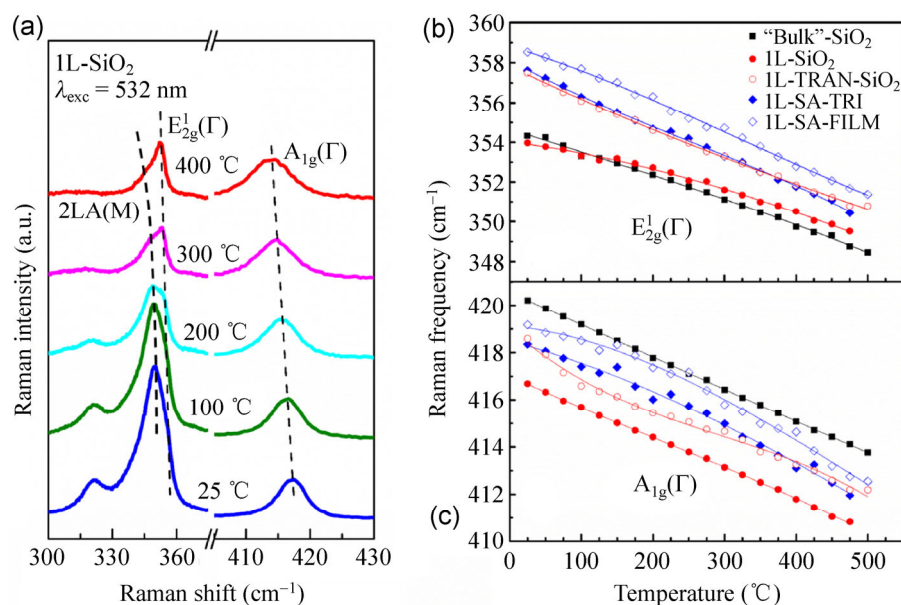


**Figure 3** (a) Representative Raman spectra of 1L-SiO<sub>2</sub> sample at different temperatures. (b)–(c) Temperature dependence of Raman frequencies of (b) E<sub>2g</sub><sup>1</sup>(Γ) and (c) A<sub>1g</sub>(Γ) modes in “bulk” and 1L samples. The solid lines are fitting results using Eq. (2), with the temperature coefficients shown in Table S1 (in the ESM).

The change in Raman frequency ( $\Delta\omega$ ) with increasing temperature typically include three contributions (Eq. (3)) [40]

$$\Delta\omega(\Delta T) = \Delta\omega_E(\Delta T) + \Delta\omega_A(\Delta T) + \Delta\omega_M(\Delta T) \quad (3)$$

where  $\Delta\omega_E$  is due to thermal expansion of the lattice, resulting in a redshift.  $\Delta\omega_A$  is attributed to anharmonic effects, i.e. phonon mode softening with increasing vibrational amplitude. The last term in Eq. (3) is related to the difference in TEC between substrate and WS<sub>2</sub>, which may introduce a strain, giving rise to a phonon frequency shift. Figures 3(b) and 3(c) show the temperature dependence of Raman frequency for both E<sub>2g</sub><sup>1</sup>(Γ) and A<sub>1g</sub>(Γ) modes in all five samples. It is common to assume that both E<sub>2g</sub><sup>1</sup>(Γ) and A<sub>1g</sub>(Γ) exhibit linear redshifts with increasing temperature. However, the clear difference in the slopes among the studied samples and the subtle non-linearity demonstrate the complexity of the film-substrate interaction.

In the case of E<sub>2g</sub><sup>1</sup>(Γ), a previous study on MoS<sub>2</sub> indicated that the transferred sample showed the least substrate effect on the in-plane mode [27]. Thus, we can take 1L-TRAN-SiO<sub>2</sub> as an approximate reference for a free-standing 1L WS<sub>2</sub>. In fact, as shown in Fig. 3(b), the temperature dependence of this sample was very

similar to the strain-free bulk MoS<sub>2</sub>, which showed a weak non-linear effect at high temperatures [27]. Other than the small variations in frequency, the temperature shifts of the two on-sapphire samples were very similar to that of the 1L-TRAN-SiO<sub>2</sub>, indicating relatively small strain in the epitaxial film and weak bonding to the substrate. However, the slopes for the two as-grown samples on SiO<sub>2</sub> were substantially less than that of 1L-TRAN-SiO<sub>2</sub>. As suggested by the RT-PL data mentioned above, 1L-SiO<sub>2</sub> is under significant tensile strain at RT, and manifests itself as the lowest Raman frequency among all the samples. Thus, the third term in Eq. (3) becomes significant. The TEC of WS<sub>2</sub> is about one order of magnitude higher than that of SiO<sub>2</sub>. With increasing temperature, the WS<sub>2</sub> film expands faster than SiO<sub>2</sub>, which in turn results in a relaxation of the tensile strain in the WS<sub>2</sub> film. The strain relaxation gives rise to a blue shift that compensates for the intrinsic red shift given by the first and the second terms in Eq. (3), resulting in a smaller temperature coefficient than those of the 1L-TRAN-SiO<sub>2</sub> and sapphire samples. This is also true for the thicker sample, “bulk”-SiO<sub>2</sub>, because it is not thick enough to allow the WS<sub>2</sub> to fully relax at RT. This explains why its temperature coefficient is higher than that of 1L-SiO<sub>2</sub>, but lower than those of the other

samples. However, because the difference in TEC between sapphire and WS<sub>2</sub> in 1L-SA-TRI and 1L-SA-FILM is small, no significant strain was generated in the films when cooled down to RT. Assuming that the transferred sample is strain free and using a DFT calculated deformation potential of  $-5.25 \text{ cm}^{-1}/\%$  under the tensile strain [42], we estimated a tensile strain of 0.67% in 1L-SiO<sub>2</sub>. The estimated values for both PL and Raman were in agreement with the value of 0.69% calculated from the TEC difference.

For A<sub>1g</sub>(Γ), the previous study on MoS<sub>2</sub> indicated that this out-of-plane mode was particularly sensitive to the film's morphology (e.g., mesoscopic scale mechanical buckling and chemical residues associated with the transferred film), and very strong non-linearity was observed for the transferred film. As shown Fig. 3(c), the strongest non-linearity was observed for the transferred film 1L-TRAN-SiO<sub>2</sub>, although it was not as significant as that reported for an ME MoS<sub>2</sub> film on SiO<sub>2</sub> [27]. The two as-grown samples on SiO<sub>2</sub> exhibited good linearity and similar slopes. Because the strain-induced A<sub>1g</sub>(Γ) frequency shift was much smaller ( $-1.94 \text{ cm}^{-1}/\%$  under tensile strain from the DFT calculation [42]) than that of E<sub>2g</sub><sup>1</sup>(Γ), the relaxation of tensile strain with increasing temperature partially offset the steeper intrinsic slope initially. This yielded linear dependence across the entire temperature range. Therefore, the intrinsic temperature coefficient for a free standing monolayer or bulk WS<sub>2</sub> is expected to be close to (but slightly larger than) that of 1L-SiO<sub>2</sub> or "bulk"-SiO<sub>2</sub>, respectively. The substrate has more influence on the results for the two on-sapphire samples than on those for the on-SiO<sub>2</sub> samples. For the transferred sample, increasing the temperature improves bonding with the substrate (e.g., evaporation of the chemical residues introduced during the film transfer), thus enhancing the charge transfer (n-type doping) from the substrate to the film [24, 25], leading to the phonon frequency red shift [28]. This effect may explain the accelerated redshift in 1L-TRAN-SiO<sub>2</sub> below 100 °C. Upon increasing the temperature further, thermally activated non-radiative recombination tends to deplete the carriers, which resulted in a less rapid temperature-dependent redshift. Above 250 °C, the temperature dependence approached that of a freestanding film. This finding suggests that an

epitaxial film has better electronic mobility than that of the transferred film, due to the difference in the symmetry selection rule for the electron-phonon coupling for the two modes. Specifically, the coupling is stronger for the A<sub>1g</sub>(Γ) mode than that for the E<sub>2g</sub><sup>1</sup>(Γ) mode [28]. This observation could help to determine the optimal thermal annealing process to achieve the desirable properties needed for use in device applications.

Based on the above discussions on the mechanisms of the phonon frequency change, fitting the experimental data assuming a linear temperature dependence is meaningful because it provides an empirical temperature dependence. Although more than one mechanism is at work, in 1L-SiO<sub>2</sub> and "bulk"-SiO<sub>2</sub>, the net effect is linear and close to that of the intrinsic WS<sub>2</sub>. For other cases, linear fitting is not justified. Nevertheless, fitting results can still illustrate significant variation with changing substrate type and bonding. We show the linear fitting results for all samples in Table 2, and the non-linear fitting results using Eq. (2) are given in Table S1 (in the ESM).

Finally, we note that the integrated Raman intensities for both E<sub>2g</sub><sup>1</sup>(Γ) and A<sub>1g</sub>(Γ) modes decreased dramatically when the temperature was > 475 °C, presumably due to the decomposition of WS<sub>2</sub> films. Upon returning to RT, the films usually could not return to their initial states. For the 1L-SiO<sub>2</sub> sample, the Raman intensities of the two phonon modes decreased to about half of their initial values. However, their peak positions remained at almost the same position as before, indicating that the bonding between the substrate and film for the CVD-grown samples was robust and not significantly altered by the annealing process. For the transferred sample, which was similar to the transferred MoS<sub>2</sub> films [27], both Raman intensities and peak positions showed significant changes. This indicates

**Table 2** Temperature coefficients of bulk and 1L WS<sub>2</sub> samples

	$\chi(E_{2g}^1(\Gamma)) \text{ (cm}^{-1}/\text{K)}$	$\chi(A_{1g}(\Gamma)) \text{ (cm}^{-1}/\text{K)}$
Bulk	$-0.0124 \pm 2 \times 10^{-4}$	$-0.0136 \pm 4 \times 10^{-5}$
1L-SiO <sub>2</sub>	$-0.0100 \pm 3 \times 10^{-4}$	$-0.0130 \pm 9 \times 10^{-5}$
1L-TRAN-SiO <sub>2</sub>	$-0.0142 \pm 1 \times 10^{-4}$	$-0.0124 \pm 4 \times 10^{-4}$
1L-SA-TRI	$-0.0154 \pm 3 \times 10^{-4}$	$-0.0140 \pm 3 \times 10^{-4}$
1L-SA-FILM	$-0.0155 \pm 2 \times 10^{-4}$	$-0.0143 \pm 6 \times 10^{-4}$

that the heating process modifies the bonding between the film and substrate, and thus changes the strain distribution across the film.

### 3.3 High-temperature photoluminescence

Lastly, we discuss the effect of temperature on PL. Figures 4(a) and 4(b) show representative PL spectra for 1L-SiO<sub>2</sub> and 1L-SA-TRI, respectively. Their peak energies are plotted in Fig. 4(c). Similar to the trends observed in Fig. 3(b) for the E<sub>2g</sub><sup>1</sup>(Γ) Raman shifts, the temperature-dependent PL peak energy shift for 1L-SiO<sub>2</sub> has a significantly smaller slope than that of 1L-SA-TRI, due to the relaxation of the built-in tensile strain for the former. The reduced slope for 1L-SA-TRI at very high temperatures (> 300 °C) is due to an increasing thermal population at higher states in the bands. The integrated PL intensities are shown in

Fig. 4(d), which indicate thermally activated temperature quenching, starting at RT. For 1L-SA-TRI, the well-known emission of Cd<sup>3+</sup> centers from the sapphire substrate has been subtracted. The experimental data can be fitted using Eq. (4) below, with one activation term for the SiO<sub>2</sub> sample (A<sub>2</sub> = 0), and two activation terms for the sapphire sample

$$I(T) = \frac{I_0}{1 + A_1 \exp(-E_{a1}/k_B T) + A_2 \exp(-E_{a2}/k_B T)} \quad (4)$$

where E<sub>a1</sub> and E<sub>a2</sub> are the activation energies of the thermal quenching processes, k<sub>B</sub> is the Boltzmann constant, I<sub>0</sub> is the integrated peak intensity at RT, and A<sub>1</sub> and A<sub>2</sub> are constants. The fitting results were as follows: for 1L-SiO<sub>2</sub>, E<sub>a1</sub> = 0.40 ± 0.01 eV; for 1L-SA-TRI, E<sub>a1</sub> = 0.20 ± 0.01 eV and E<sub>a2</sub> = 1.51 ± 0.06 eV, respectively, with the fitting curves shown in Fig. 4(d). Temperature

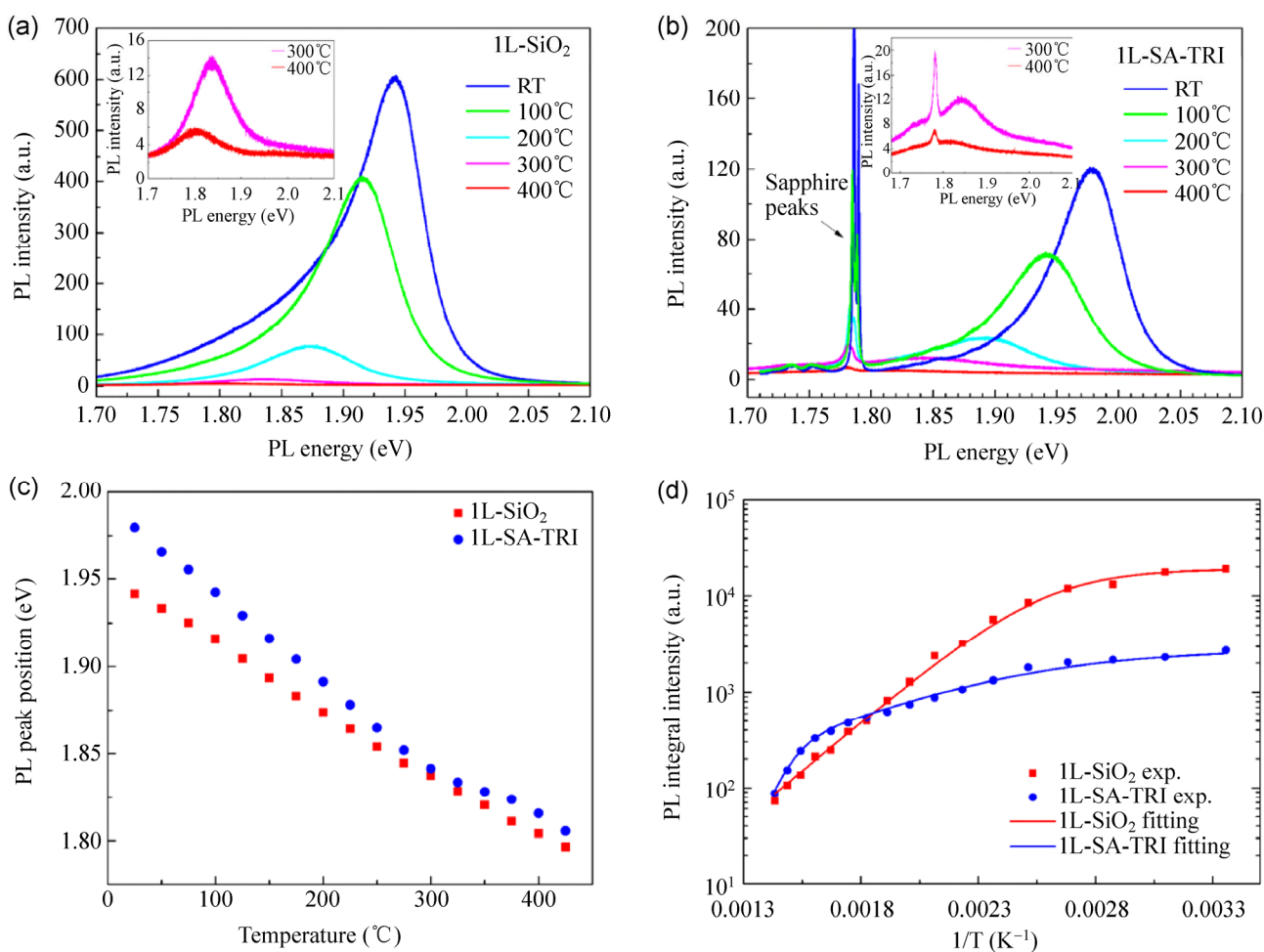


**Figure 4** (a)–(b) Representative PL spectra of (a) 1L-SiO<sub>2</sub> and (b) 1L-SA-TRI at particular temperatures. (c) Temperature dependence of PL peak energy for 1L-SiO<sub>2</sub> and 1L-SA-TRI samples. (d) Integral PL intensity of 1L-SiO<sub>2</sub> and 1L-SA-TRI at different temperatures.

induced PL quenching in semiconductors typically results from direct or indirect thermal activation of non-radiative recombination processes associated with defects or impurities through emission of phonons. Activation energies as large as these values are unusual. This is because PL is rarely performed at temperatures much higher than RT to assess the potential process with such a large activation energy. Our current understanding of defects and impurities in these 2D materials is very limited. Thus, speculating on the physical origins of these thermal quenching processes is premature. However, an important issue for 2D materials is the interfacial effect involving carrier exchange between the 2D film and the substrate through the thermal activation process. In fact, the magnitudes of the activation energies are comparable to the possible energy barriers between the film and the substrate. Theoretical modeling based on first-principle techniques is needed to understand the film-substrate interactions that yielded the effects reported in this study. This will further our understanding of the electronic and vibrational properties of 2D materials.

#### 4 Conclusions

In summary, we performed high-temperature (25–500 °C) Raman and PL studies on CVD-grown epitaxial monolayer WS<sub>2</sub> on SiO<sub>2</sub>/Si and sapphire substrates. The interaction between the 2D film and substrate was shown to depend on substrate type for the as-grown samples and film-substrate bonding between the as-grown and the transferred samples. At RT, the PL intensity of monolayer WS<sub>2</sub> on SiO<sub>2</sub> was found to be much stronger than that on the sapphire substrate under both 532 and 441.6 nm excitation. The TEC mismatch between the thin-film and SiO<sub>2</sub>/Si substrate generated a significant amount of strain after the film was cooled down to RT, manifesting itself as a bandgap shift, strong intensity modification in resonant Raman scattering, and large non-linearity in the temperature coefficient of the vibration mode frequency. The effects were minimal for the sapphire substrate. These effects, which are associated with the built-in strain, are inherent properties of the directly grown 2D films. However, this depended upon the specific substrate

used. A significant difference existed in the states of the built-in strain between the directly grown and the transferred films, even on the same type of substrate. The in-plane vibration mode, E<sub>2g</sub><sup>1</sup>(Γ), was more sensitive to the strain effect, whereas the out-of-plane vibration mode, A<sub>1g</sub>(Γ), was more sensitive to the film-substrate bonding or the film morphology. Because of the strong electron-phonon coupling of the A<sub>1g</sub>(Γ) mode as dictated by symmetry, a transferred film without proper thermal annealing was expected to have an inferior carrier mobility. The intrinsic temperature coefficients for the E<sub>2g</sub><sup>1</sup>(Γ) and A<sub>1g</sub>(Γ) modes in monolayer WS<sub>2</sub> were determined to be:  $\chi(E_{2g}^1(\Gamma)) = -0.0142 \pm 2 \times 10^{-4} \text{ cm}^{-1}/\text{K}$ , derived from the transferred film on SiO<sub>2</sub>; and  $\chi(A_{1g}(\Gamma)) = -0.0130 \pm 9 \times 10^{-5} \text{ cm}^{-1}/\text{K}$  (lower bound), derived from the as-grown film on SiO<sub>2</sub>. These values were somewhat smaller than the corresponding ones in MoS<sub>2</sub>:  $\chi(E_{2g}^1(\Gamma)) = -0.0221 \pm 9 \times 10^{-4} \text{ cm}^{-1}/\text{K}$ , and  $\chi(A_{1g}(\Gamma)) = -0.0197 \pm 9 \times 10^{-4} \text{ cm}^{-1}/\text{K}$  [27]. For all other cases, the temperature coefficients were affected by the substrate to different extents, but this effect was most severe for the film grown on SiO<sub>2</sub> with  $\chi(E_{2g}^1(\Gamma)) = -0.0100 \pm 3 \times 10^{-4} \text{ cm}^{-1}/\text{K}$ . Therefore, the temperature-dependent Raman investigations provided an effective tool for investigating the epilayer-substrate interaction. Additionally, high-temperature PL studies on monolayer WS<sub>2</sub> revealed thermal quenching processes with large activation energies of  $E_{a1} = 0.40 \text{ eV}$  for the film grown on SiO<sub>2</sub> and  $E_{a1} = 0.20 \text{ eV}$  and  $E_{a2} = 1.51 \text{ eV}$  for the film grown on sapphire.

#### Acknowledgements

Y. Z. acknowledges the support of Bissell Distinguished Professorship. L. Y. C. acknowledges the support of a Young Investigator Award from the Army Research Office (No. W911NF-13-1-0201).

**Electronic Supplementary Material:** Supplementary material (Raman spectrum fitting, PL spectra collected with 532 nm excitation wavelength, Raman spectrum correction of 1L WS<sub>2</sub> on sapphire, and temperature coefficients for all samples fitted with a third-order polynomial function) is available in the online version of this article at <http://dx.doi.org/10.1007/s12274-015-0775-1>.

## References

- [1] Novoselov, K. S.; Geim, A. K.; Morozov, S. V.; Jiang, D.; Zhang, Y.; Dubonos, S. V.; Grigorieva, I. V.; Firsov, A. A. Electric field effect in atomically thin carbon films. *Science* **2004**, *306*, 666–669.
- [2] Geim, A. K.; Novoselov, K. S. The rise of graphene. *Nat. Mater.* **2007**, *6*, 183–191.
- [3] Jin, C.; Lin, F.; Suenaga, K.; Iijima, S. Fabrication of a freestanding boron nitride single layer and its defect assignments. *Phys. Rev. Lett.* **2009**, *102*, 195505.
- [4] Ci, L. J.; Song, L.; Jin, C. H.; Jariwala, D.; Wu, D. X.; Li, Y. J.; Srivastava, A.; Wang, Z. F.; Storr, K.; Balicas, L. et al. Atomic layers of hybridized boron nitride and graphene domains. *Nat. Mater.* **2010**, *9*, 430–435.
- [5] Schutte, W. J.; De Boer, J. L.; Jellinek, F. Crystal-structures of tungsten disulfide and diselenide. *J. Solid State Chem.* **1987**, *70*, 207–209.
- [6] Ramakrishna Matte, H. S. S.; Gomathi, A.; Manna, A. K.; Late, D. J.; Datta, R.; Pati, S. K.; Rao, C. N. R. MoS<sub>2</sub> and WS<sub>2</sub> analogues of graphene. *Angew. Chem. Int. Ed.* **2010**, *122*, 4153–4156.
- [7] Splendiani, A.; Sun, L.; Zhang, Y. B.; Li, T. S.; Kim, J.; Chim, C. Y.; Galli, G.; Wang, F. Emerging photoluminescence in monolayer MoS<sub>2</sub>. *Nano Lett.* **2010**, *10*, 1271–1275.
- [8] Mak, K. F.; Lee, C.; Hone, J.; Shan, J.; Heinz, T. F. Atomically thin MoS<sub>2</sub>: A new direct-gap semiconductor. *Phys. Rev. Lett.* **2010**, *105*, 136805.
- [9] Eda, G.; Yamaguchi, H.; Voiry, D.; Fujita, T.; Chen, M.; Chhowalla, M. Photoluminescence from chemically exfoliated MoS<sub>2</sub>. *Nano Lett.* **2011**, *11*, 5111–5116.
- [10] Albe, K.; Klein, A. Density-functional-theory calculations of electronic band structure of single-crystal and single-layer WS<sub>2</sub>. *Phys. Rev. B* **2002**, *66*, 073413.
- [11] Wang, Q. H.; Kalantar-Zadeh, K.; Kis, A.; Coleman, J. N.; Strano, M. S. Electronics and optoelectronics of two-dimensional transition metal dichalcogenides. *Nat. Nano.* **2012**, *7*, 699–712.
- [12] Gutiérrez, H. R.; Perea-López, N.; Elías, A. L.; Berkdemir, A.; Wang, B.; Lv, R.; López-Urías, F.; Crespi, V. H.; Terrones, H.; Terrones, M. Extraordinary room-temperature photoluminescence in triangular WS<sub>2</sub> monolayers. *Nano Lett.* **2012**, *13*, 3447–3454.
- [13] Zhao, W. J.; Ghorannevis, Z.; Chu, L. Q.; Toh, M.; Kloc, C.; Tan, P. H.; Eda, G. Evolution of electronic structure in atomically thin sheets of WS<sub>2</sub> and WSe<sub>2</sub>. *ACS Nano* **2012**, *7*, 791–797.
- [14] Yun, W. S.; Han, S. W.; Hong, S. C.; Kim, I. G.; Lee, J. D. Thickness and strain effects on electronic structures of transition metal dichalcogenides: 2H-MX<sub>2</sub> semiconductors ( $M = \text{Mo}, \text{W}; X = \text{S}, \text{Se}, \text{Te}$ ). *Phys. Rev. B* **2012**, *85*, 033305.
- [15] Zhao, W. J.; Ghorannevis, Z.; Amara, K. K.; Pang, J. R.; Toh, M.; Zhang, X.; Kloc, C.; Tan, P. H.; Eda, G. Lattice dynamics in mono- and few-layer sheets of WS<sub>2</sub> and WSe<sub>2</sub>. *Nanoscale* **2013**, *5*, 9677–9683.
- [16] Tonndorf, P.; Schmidt, R.; Böttger, P.; Zhang, X.; Börner, J.; Liebig, A.; Albrecht, M.; Kloc, C.; Gordan, O.; Zahn, D. R. T. et al. Photoluminescence emission and Raman response of monolayer MoS<sub>2</sub>, MoSe<sub>2</sub>, and WSe<sub>2</sub>. *Opt. Express* **2013**, *21*, 4908–4916.
- [17] Radisavljevic, B.; Radenovic, A.; Brivio, J.; Giacometti, V.; Kis, A. Single-layer MoS<sub>2</sub> transistors. *Nat. Nano.* **2011**, *6*, 147–150.
- [18] Mak, K. F.; He, K.; Shan, J.; Heinz, T. F. Control of valley polarization in monolayer MoS<sub>2</sub> by optical helicity. *Nat. Nano.* **2012**, *7*, 494–498.
- [19] Zeng, H. L.; Dai, J. F.; Yao, W.; Xiao, D.; Cui, X. D. Valley polarization in MoS<sub>2</sub> monolayers by optical pumping. *Nat. Nano.* **2012**, *7*, 490–493.
- [20] Mao, X. Z.; Xu, Y.; Xue, Q. X.; Wang, W. X.; Gao, D. Q. Ferromagnetism in exfoliated tungsten disulfide nanosheets. *Nanoscale Res. Lett.* **2013**, *8*, 430.
- [21] Zhou, Y. G.; Su, Q. L.; Wang, Z. G.; Deng, H. Q.; Zu, X. T. Controlling magnetism of MoS<sub>2</sub> sheets by embedding transition-metal atoms and applying strain. *Phys. Chem. Chem. Phys.* **2013**, *15*, 18464–18470.
- [22] Georgiou, T.; Jalil, R.; Belle, B. D.; Britnell, L.; Gorbachev, R. V.; Morozov, S. V.; Kim, Y. J.; Gholinia, A.; Haigh, S. J.; Makarovskiy, O. et al. Vertical field-effect transistor based on graphene-WS<sub>2</sub> heterostructures for flexible and transparent electronics. *Nat. Nano.* **2013**, *8*, 100–103.
- [23] Britnell, L.; Ribeiro, R. M.; Eckmann, A.; Jalil, R.; Belle, B. D.; Mishchenko, A.; Kim, Y. J.; Gorbachev, R. V.; Georgiou, T.; Morozov, S. V. et al. Strong light-matter interactions in heterostructures of atomically thin films. *Science* **2013**, *340*, 1311–1314.
- [24] Scheuschner, N.; Ochedowski, O.; Kaulitz, A. M.; Gillen, R.; Schleberger, M.; Maultzsch, J. Photoluminescence of freestanding single- and few-layer MoS<sub>2</sub>. *Phys. Rev. B* **2014**, *89*, 125406.
- [25] Sercombe, D.; Schwarz, S.; Pozo-Zamudio, O. D.; Liu, F.; Robinson, B. J.; Chekhovich, E. A.; Tartakovskii, I. I.; Kolosov, O.; Tartakovskii, A. I. Optical investigation of the natural electron doping in thin MoS<sub>2</sub> films deposited on dielectric substrates. *Sci. Rep.* **2013**, *3*, 3489.
- [26] Buscema, M.; Steele, G.; van der Zant, H. S. J.; Castellanos-Gomez, A. The effect of the substrate on the Raman and photoluminescence emission of single-layer MoS<sub>2</sub>. *Nano Res.* **2014**, *7*, 1–11.

- [27] Su, L. Q.; Zhang, Y.; Yu, Y. F.; Cao, L. Y. Dependence of coupling of quasi 2-D MoS<sub>2</sub> with substrates on substrate types, probed by temperature dependent Raman scattering. *Nanoscale* **2014**, *6*, 4920–4927.
- [28] Chakraborty, B.; Bera, A.; Muthu, D. V. S.; Bhowmick, S.; Waghmare, U. V.; Sood, A. K. Symmetry-dependent phonon renormalization in monolayer MoS<sub>2</sub> transistor. *Phys. Rev. B* **2012**, *85*, 161403.
- [29] Calizo, I.; Balandin, A. A.; Bao, W.; Miao, F.; Lau, C. N. Temperature dependence of the Raman spectra of graphene and graphene multilayers. *Nano Lett.* **2007**, *7*, 2645–2649.
- [30] Molina-Sánchez, A.; Wirtz, L. Phonons in single-layer and few-layer MoS<sub>2</sub> and WS<sub>2</sub>. *Phys. Rev. B* **2011**, *84*, 155413.
- [31] Berkdemir, A.; Gutierrez, H. R.; Botello-Mendez, A. R.; Perea-Lopez, N.; Elias, A. L.; Chia, C. I.; Wang, B.; Crespi, V. H.; Lopez-Urias, F.; Charlier, J. C. et al. Identification of individual and few layers of WS<sub>2</sub> using Raman spectroscopy. *Sci. Rep.* **2013**, *3*, 1755.
- [32] Ishigami, M.; Chen, J. H.; Cullen, W. G.; Fuhrer, M. S.; Williams, E. D. Atomic structure of graphene on SiO<sub>2</sub>. *Nano Lett.* **2007**, *7*, 1643–1648.
- [33] Lin, Y. C.; Lu, C. C.; Yeh, C. H.; Jin, C.; Suenaga, K.; Chiu, P. W. Graphene annealing: How clean can it be? *Nano Lett.* **2011**, *12*, 414–419.
- [34] Yu, Y. F.; Hu, S.; Su, L. Q.; Huang, L. J.; Liu, Y.; Jin, Z. H.; Puzosky, A. A.; Geohegan, D. B.; Kim, K. W.; Zhang, Y. et al. Equally efficient interlayer exciton relaxation and improved absorption in epitaxial and nonepitaxial MoS<sub>2</sub>/WS<sub>2</sub> heterostructures. *Nano Lett.* **2015**, *15*, 486–491.
- [35] Gurarslan, A.; Yu, Y. F.; Su, L. Q.; Yu, Y. L.; Suarez, F.; Yao, S. S.; Zhu, Y.; Ozturk, M.; Zhang, Y.; Cao, L. Y. Surface-energy-assisted perfect transfer of centimeter-scale monolayer and few-layer MoS<sub>2</sub> films onto arbitrary substrates. *ACS Nano* **2014**, *8*, 11522–11528.
- [36] Elías, A. L.; Perea-López, N.; Castro-Beltrán, A.; Berkdemir, A.; Lv, R.; Feng, S.; Long, A. D.; Hayashi, T.; Kim, Y. A.; Endo, M. et al. Controlled synthesis and transfer of large-area WS<sub>2</sub> sheets: From single layer to few layers. *ACS Nano* **2013**, *7*, 5235–5242.
- [37] Ballif, C.; Regula, M.; Schmid, P. E.; Remškar, M.; Sanjinés, R.; Lévy, F. Preparation and characterization of highly oriented, photoconducting WS<sub>2</sub> thin films. *Appl. Phys. A* **1996**, *62*, 543–546.
- [38] Peimyoo, N.; Yang, W. H.; Shang, J. Z.; Shen, X. N.; Wang, Y. L.; Yu, T. Chemically driven tunable light emission of charged and neutral excitons in monolayer WS<sub>2</sub>. *ACS Nano* **2014**, *8*, 11320–11329.
- [39] Mak, K. F.; He, K.; Lee, C.; Lee, G. H.; Hone, J.; Heinz, T. F.; Shan, J. Tightly bound trions in monolayer MoS<sub>2</sub>. *Nat. Mater.* **2013**, *12*, 207–211.
- [40] Yoon, D.; Son, Y. W.; Cheong, H. Negative thermal expansion coefficient of graphene measured by Raman spectroscopy. *Nano Lett.* **2011**, *11*, 3227–3231.
- [41] Matthäus, A.; Ennaoui, A.; Fiechter, S.; Tiefenbacher, S.; Kiesewetter, T.; Diesner, K.; Sieber, I.; Jaegermann, W.; Tsirlina, T.; Tenne, R. Highly textured films of layered metal disulfide 2H-WS<sub>2</sub>: Preparation and optoelectronic properties. *J. Electrochem. Soc.* **1997**, *144*, 1013–1019.
- [42] Li, Y.; Wang, J. W.; Li, J. B.; Zhang, Y. Unpublished work, 2015.
- [43] Ling, X.; Moura, L. G.; Pimenta, M. A.; Zhang, J. Charge-transfer mechanism in graphene-enhanced Raman scattering. *J. Phys. Chem. C* **2012**, *116*, 25112–25118.
- [44] M., T.; Late, D. J. Temperature dependent phonon shifts in single-layer WS<sub>2</sub>. *ACS Appl. Mater. Inter.* **2013**, *6*, 1158–1163.
- [45] Dumcenco, D.; Ovchinnikov, D.; Marinov, K.; Lopez-Sanchez, O.; Krasnozhan, D.; Chen, M. W.; Gillet, P.; Morral, A. F. i.; Radenovic, A.; Kis, A. Large-area epitaxial monolayer MoS<sub>2</sub>. *ArXiv e-prints* [Online] **2014**, 129. <http://adsabs.harvard.edu/abs/2014arXiv1405.0129D> (accessed Jan 22, 2015).